6th European Conference on Computational Mechanics (ECCM 6)
7th European Conference on Computational Fluid Dynamics (ECFD 7)
11-15 June 2018, Glasgow, UK

FINITE ELEMENT ANALYSIS AND FAILURE PREDICTION OF ADHESIVE JOINTS IN WIND TURBINE ROTOR BLADES

CLAUDIO BALZANI[1], PABLO NOEVER-CASTELOS[1] AND MICHAEL WENTINGMANN[1]

[1] Leibniz Universität Hannover, Institute for Wind Energy Systems
Appelstraße 9A, 30167 Hannover, Germany
research@iwes.uni-hannover.de
www.iwes.uni-hannover.de

Key words: Failure, Fatigue, Adhesive, Finite Element, Wind Turbine, Rotor Blade

Abstract. Wind turbines have been growing in size significantly during the past years. As a consequence, the mechanical loads acting on the wind turbine components increase as well. This gives rise to the need to develop new or to enhance existing methodologies for failure analyses of wind turbine components. This paper deals with the finite element analysis of adhesive joints in wind turbine rotor blades and addresses both ultimate and fatigue load analyses.

For ultimate loading, an equivalent stress approach is utilized. In fatigue, wind turbines experience high amplitudes and very high cycle numbers. Hence, an appropriate fatigue analysis framework is of utmost importance. In this paper a critical plane approach is employed. The model captures multiaxial stress states as required by current design guidelines and takes into account non-proportional stress histories.

The paper focuses on the trailing edge adhesive joints, as they are highly stressed in longitudinal direction and shear. Representative numerical examples show that a multiaxial strength analysis for ultimate and fatigue loads is extraordinarily important to design reliable adhesive joints. The necessity to account for non-proportionality in the stress histories is also demonstrated.

1 INTRODUCTION

There is an ongoing trend in the wind energy industry of turbine upscaling. Today, the largest rotor blade has a length of 88.4 m, which makes it the largest one-piece engineering structure in the world. Such structures are prone to massive mechanical loads that are originated by complex loading states with contributions of the rotating dead loads in operation, the aerodynamic forces, the inertial forces, wind shear, turbulence, etc. Wind turbine rotor blades experience extraordinarily high load amplitudes and suffer from very high cycle fatigue with cycle numbers of up to 10^8–10^9. It is clear that for such structures the risk of material damages increases dramatically. Hence, applicable and

accurate simulation and analysis procedures are required that enable engineers to design robust and reliable rotor blades for future generation wind turbines.

Design standards and guidelines [1–3] are available that help engineers to choose analysis procedures. In the 2010 edition of Germanischer Lloyd [2] a uniaxial shear stress proof was required for the certification of adhesive joints in rotor blades. However, e.g. the trailing edge adhesive joint is significantly stressed by longitudinal strains. Hence, the current edition of DNV-GL [3] demands a three-dimensional stress proof. However, no indication is given which method to apply to accomplish this requirement. There is also only little literature available [4–9] that studies simulation methodologies for the design of adhesive joints in wind turbine rotor blades.

In this paper, we propose one possible strategy how to perform a stress analysis of adhesive joints in wind turbine rotor blades fulfilling the needs of current design guidelines. For the analysis of ultimate stress states, we employ an equivalent stress approach based on the Drucker-Prager theory [10]. In this way we take into account three-dimensional stress states and different tensile and compressive strength parameters. However, an equivalent stress approach cannot be utilised for a fatigue analysis due to a couple of reasons that will be pointed out in this paper. Several fatigue analysis concepts are described in literature, most of which included in [11–14]. The *critical plane approach* combined with Miner's rule [15] is a promising methodology, as it is able to capture non-proportional stress histories that are present in wind turbine rotor blades. Since it is also suggested for metallic parts in wind turbines under non-proportional multiaxial stress states [2], we adopt this method for adhesive joints. A representative example of a virtual state-of-the-art wind turbine rotor blade shows the applicability of the proposed concept.

2 FINITE ELEMENT MODEL

The aim is to analyse a rotor blade by means of 3D finite element (FE) analyses. In order to derive an FE model of a rotor blade, the inhouse **Mo**del **C**reator and **A**nalysis Tool MoCA is utilised. MoCA is based on a full parameterisation of a blade and creates FE models for ANSYS [16]. The geometry of a finite number of cross-sections is normally defined in the framework of a blade design procedure. In between, the nodal positions of the 3D geometry is interpolated by piecewise cubic splines.

The structural members consisting of fiber composites or sandwich panels, i.e. the spar caps, the shear webs, and the shells, are modelled with quadrilateral shell elements (element type number 181). The trailing edge adhesive joint is discretised by 8-noded solid elements (element type number 185). Figure 1 shows an example FE mesh of a rotor blade as a result of MoCA and a detail of the trailing edge adhesive joint.

The translational and rotational degrees of freedom are fixed at the blade root. The introduction of the loads acting on the blade is realised according to the methodology described in [8]. Therein, multiple point constraints (MPCs) are used for the application of forces and moments (element type number 170 for the target node and element number 177 for the contact nodes). Coupled aero-servo-elastic turbine simulations are the basis for the force-like boundary conditions. We used HAWC2 [17] for such turbine simulations that capture the turbine dynamics and give us the internal forces and moments in the

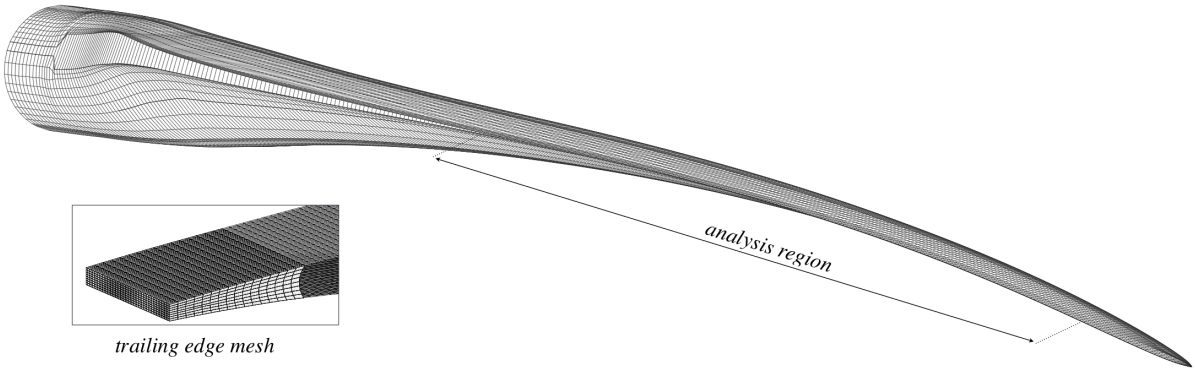

Figure 1: Finite element mesh of a wind turbine rotor blade generated with MoCA, an inhouse model creator. The rotor blade length is 80 m. The trailing edge adhesive joint was implemented in the marked analysis region (span from 34–74 m). A detailed view of the trailing edge mesh is presented on the left.

blade. The 3D FE model is then utilised for transferring the internal loads into the stress space. In this way, we give the structure of the blade more flexibility, as the cross-sections are allowed to deform, a feature not included in beam model-based turbine simulations.

3 STRENGTH ANALYSIS METHODOLOGY

In this section we describe a methodology for static strength and fatigue damage analyses of adhesive joints in wind turbine rotor blades.

3.1 Static strength analysis

For the assessment of the static strength of the adhesive joint, we perform a *worst case analysis*. Therein we apply all ultimate loads along the blade in one analysis. According to [1,2] several design load cases (DLC) have to be analysed by means of turbine simulations. In each DLC, many different wind speeds, inflow inclinations, etc. have to be accounted for. This means that there are tens to hundreds of time series, each of which 600 seconds long with time steps of about 0.01 seconds. In these time series, we search for the maximum internal loads along the blades. The distribution of internal loads is then approximated by application of corresponding external loads in the 3D FE model.

The 3D FE simulation is carried out including geometric nonlinearities (large deflections). The stress results in the adhesive joints are saved in a results file. Those results are transferred to a postprocessor that is also implemented in the MoCA package. Therein, we evaluate the three-dimensional stress states in the adhesive by means of stress-strength relationships. We apply the well-known Drucker-Prager equivalent stress, see [10], which is calculated by the expression

$$\sigma_v = \frac{m-1}{2}\left(\sigma_1+\sigma_2+\sigma_3\right) + \frac{m+1}{2}\sqrt{\frac{1}{2}\left[\left(\sigma_1-\sigma_2\right)^2+\left(\sigma_2-\sigma_3\right)^2+\left(\sigma_3-\sigma_1\right)^2\right]}\,. \qquad (1)$$

Herein, m is defined as the ratio between the tensile strength, R_t, and the compressive strength, R_c, i.e. $m := R_t/R_c$. In (1), σ_1, σ_2, and σ_3 are the principal stresses extracted from the 3D FE simulation. For the principal stresses the convention $\sigma_1 \geq \sigma_2 \geq \sigma_3$

holds. The strength ratio m normalises the principal stresses to the tensile strength. The equivalent stress approach reduces the three-dimensional stress state to a one-dimensional magnitude that makes the model easy to handle. Besides, the Drucker-Prager theory enables us to account for different tensile and compressive normal strengths, as is the case for adhesives in wind turbine rotor blades. However, the accuracy of the Drucker-Prager theory for wind turbine adhesives needs to be validated by experimental investigations.

3.2 Fatigue analysis

A fatigue strength analysis is much more complex than an ultimate stress analysis. Again, the design standards [1, 2] demand several DLCs that are relevant for fatigue failure. In each DLC, several time series need to be simulated. Each time series has to be treated completely in order to extract the number of cycles and the corresponding amplitudes and mean stress levels. This results in thousands of time steps that need to be transferred to the stress space.

In order not to perform transient analyses with the 3D FE model, we employ the concept of superposition of scaled unit load cases, see also [8]. Therein, we perform one unit load analysis on the 3D model for each internal load component and calculate the stresses in the adhesive joint. Then, we scale the unit load stresses by the actual loads, and superimpose the influences of the different internal load components. In this way we calculate the stress histories of the adhesive joint with minimum computational cost.

Once we have the stress time histories, we have to calculate the fatigue damage. There are several publications that deal with fatigue analyses of structures, and different calculation strategies are available, see e.g. [11–14]. We follow Miner's rule [15] of linear damage accumulation given by

$$D = \sum_{i=1}^{n} D_i = \sum_{i=1}^{n} \frac{n_i}{N_i} \,, \tag{2}$$

where D is the fatigue damage, i denotes a specific combination of stress amplitude and mean stress, n is the total number of stress amplitude/mean stress combinations, D_i is the partial fatigue damage for the specific stress amplitude/mean stress combination i, n_i is the number of cycles for the particular stress amplitude/mean stress combination i, and N_i is the corresponding maximum allowable of the number of cycles. A fatigue crack occurs if for the fatigue damage it holds $D > 1$.

The maximum allowable cycle number for a stress amplitude/mean stress combination can be taken from S-N-curves, that give the material strength as a function of the cycle number for a particular stress amplitude/mean stress combination. The S-N-curves are material-specific and have to be determined experimentally.

For the calculation of the partial damages, we need to apply a rainflow counting scheme [18] to the stress histories in order to create a stress collective that assigns the number of cycles to the different stress amplitude/mean stress combinations.

The question remains which stress to include in the rainflow count and in the analysis of the partial damages. Most equivalent stress aproaches cannot capture non-proportional stress histories and accumulate damages that appear on different material planes. Rotor

blades are exposed to a combination of deterministic loadings (e.g. due to rotating dead weights or the wind shear) and stochastic loadings (e.g. due to turbulences in the wind field). It is thus obvious that due to the combination of these two load types, the stress history is non-proportional, i.e. the direction of the principal stress is changing with time. An equivalent stress is a scalar-valued magnitude that does not have a direction. Hence, a change in stress direction is not taken into account. As a side effect, all damages are accumulated, no matter on which material plane the stresses are acting on. This is physically not meaningful. Hence, we propose a critical plane approach, see e.g. [11–14], which is described in the next paragraph. Besides, the critical plane approach gives the orientation of an initial fatigue crack, which is a good starting point for fracture mechanics-based crack propagation analyses.

In a critical plane approach, the stress time history is projected onto the particular plane of interest, reducing the stress tensors to traction vectors with one normal traction and two shear tractions. We filter small amplitudes in the traction time history via a multiaxial racetrack filter [19] in order to improve the computational efficiency of the modified Wang-Brown (MWB) rainflow counting scheme [20] that is applied afterwards. The MWB scheme accounts for multiaxial stress histories as present here. The stress amplitudes are subsequently calculated via a polar moment of inertia method described in [21–23]. The Findley damage criterion [24] is utilised for the calculation of fatigue damage in combination with the linear damage accumulation given in (2). The material plane with the maximum damage is interpreted as the critical plane on which a crack will actually initiate. A computationally very efficient way to identify the critical plane based on half sphere discretisations [25] is given in [26].

The fatigue damage is calculated for each wind speed time series of 600 seconds. The wind speed frequency normally follows a Weibull distribution. Hence, the fatigue damages are subsequently extrapolated via such Weibull distribution in order to obtain the annual fatigue damage on each plane.

The model seems to be physically meaningful and thus accurate and applicable. However, we would like to emphasize that the accuracy of the model needs to be validated by experimental investigations in the near future.

4 APPLICATION EXAMPLE

This section presents a representative numerical example that demonstrates the applicability of the proposed concept. The analyses are carried out for the trailing edge adhesive joint of the reference rotor blade [27] of the IWT-7.5-164 reference turbine model [28]. The rotor blade has a length of 80 m and a prebend at the tip of 4.5 m. It is composed of a carbon/epoxy fiber composite spar cap, two shear webs of sandwich material with foam core and glass/epoxy facesheets, and a shell of sandwich panels with foam core and glass/epoxy facesheets. At the maximum chord position, a third shear web is introduced. The adhesive joint consists of an epoxy-based adhesive. The adhesive joint was not dimensioned in [27,28]. Hence, we assume a width of the joint of 10 cm. We further assume a concave inner face shape of the joint.

4.1 Static strength analysis

We analyse a region along the span between 41 m and 47 m. The load introduction is realised as described in [9] by cutting the blade at a span of 54 m and applying the internal forces and moments from the turbine simulation (which were previously interpolated in a linear fashion) at a span position between 53 m and 54 m. For this purpose rigid multiple point constraints (element type number 170 for the target node and element type number 177 for the contact nodes; the target node is located at the threading line of the profiles) were utilised. In the cross-sections, the load is distributed along the blade's shell. The loads applied to the 3D FE model are slightly conservative, but generally in quite good agreement with the turbine simulations, see also [9].

The characteristic tensile, compressive, and shear strength values used for the simulations are given in Tab. 1. These were adopted from [29]. Note that the compressive strength is considerably larger than the tensile strength, and that the shear strength is almost half as much as the tensile strength. For the calculation of the material design values we take into account a partial safety factor of $\gamma_{\mathrm{Md}} = 2.45$, and for the loads we use a partial safety factor of $\gamma_{\mathrm{F}} = 1.35$, both see [2].

Table 1: Average characteristic strength values of the adhesive adopted from [29].

Tensile strength	Compressive strength	Shear strength
41.95 MPa	75.30 MPa	19.92 MPa

The results of the simulations are shown in Fig. 2, where we plot several stresses against the spanwise position in the stress evaluation area. Therein, the graph marked 'Drucker-Prager' is calculated according to (1). The graph marked 'Tresca' is the maximum shear equivalent stress according to Tresca, see e.g. [30]. The graphs $\tau_{\mathrm{xz,GL}}$ and $\tau_{\mathrm{yz,GL}}$ are calculated according to a simplified method proposed in [31], which is not further discussed in the following. Details can be found in [9]. The design tensile strength and the design shear strength are denoted by $R_{t,d}$ and $R_{s,d}$, respectively, while $R_{s,d,GL}$ denotes the design shear strength of an adhesive certified by Germanischer Lloyd, see [2]. For the Drucker-Prager and the Tresca results, we included the bandwidth of three times the standard deviation of values in the respective cross-section.

Interestingly, we observe a sudden increase of equivalent stress at a span of approximately 45.5 m, no matter if the Drucker-Prager or the Tresca criterion is used. This increase is originated from ply drop-offs in the trailing edge spar, which leads to an increase of strain (and consequently of stress) in the trailing edge adhesive joint. From that it follows that strengthening the trailing edge spar can help in dimensioning a trailing edge adhesive joint.

We further observe that the Tresca equivalent stress, which is a uniaxial shear criterion, exceeds the design shear strength at some spanwise positions. This means that when we only account for shear stresses, as for instance required due to older design guidelines [2], we do not fulfill the stress proof. If we utilise the Drucker-Prager equivalent stress,

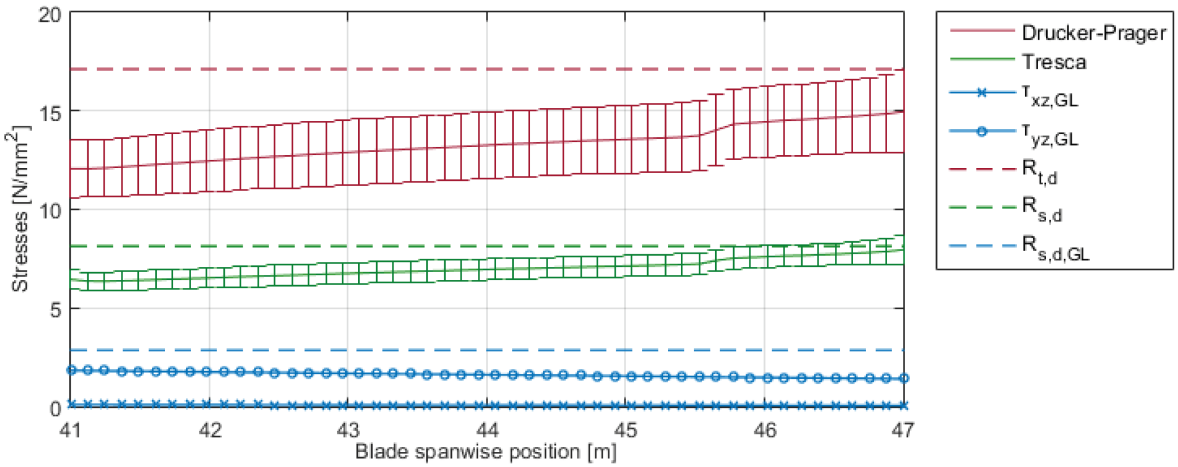

Figure 2: Stresses plotted against the spanwise position of the blade ('Drucker-Prager' is the equivalent stress according to (1); 'Tresca' is the Tresca equivalent stress, see [30]; $\tau_{\mathrm{xz,GL}}$ and $\tau_{\mathrm{yz,GL}}$ are calculated according to a simplified method proposed in [31]; $R_{t,d}$ and $R_{s,d}$ are the design tensile and shear strength according to [29]; $R_{s,d,GL}$ is the design shear strength for an adhesive certified by GL according to [2]).

the stress proof is generally fulfilled. Since the Drucker-Prager approach accounts for complete three-dimensional stress states, it is more general then the Tresca approach (and potentially more accurate), and fulfills current requirements of the design guidelines [3].

4.2 Fatigue analysis

In this section we present the results of the fatigue analysis. The fatigue damage is evaluated in five evaluation regions denoted by $\mathcal{A}_1$–$\mathcal{A}_5$. The evaluation regions are located between load introduction positions. There is sufficient distance between the load introduction and stress evaluation regions, so that the displacment field in the adhesive (and consequently the strain and stress fields) do not suffer from displacement constraints introduced by the load introduction. The specific locations of the evaluation regions in spanwise direction are given in Tab. 2. In the evaluation regions, the FE mesh is locally refined. In each refined region, $32 \times 16 \times 8$ elements are used in spanwise direction, chordwise direction, and thickness direction, respectively.

Table 2: Spanwise positions of the fatigue evaluation regions $\mathcal{A}_1$–$\mathcal{A}_5$.

Evaluation region	$\mathcal{A}_1$	$\mathcal{A}_2$	$\mathcal{A}_3$	$\mathcal{A}_4$	$\mathcal{A}_5$
Spanwise position (in m)	36.5–37.5	45.5–46.5	54.5–55.5	63.4–64.4	72.4–73.3

Figure 3 shows the results of the fatigue analysis for all evaluation regions. The damage extrapolation for the calculation of the annual damage is based on a Weibull distribution of the wind speed frequency with a shape factor of 2. We have included the normal operation DLC from [2]. This DLC includes different wind speeds, six different seed

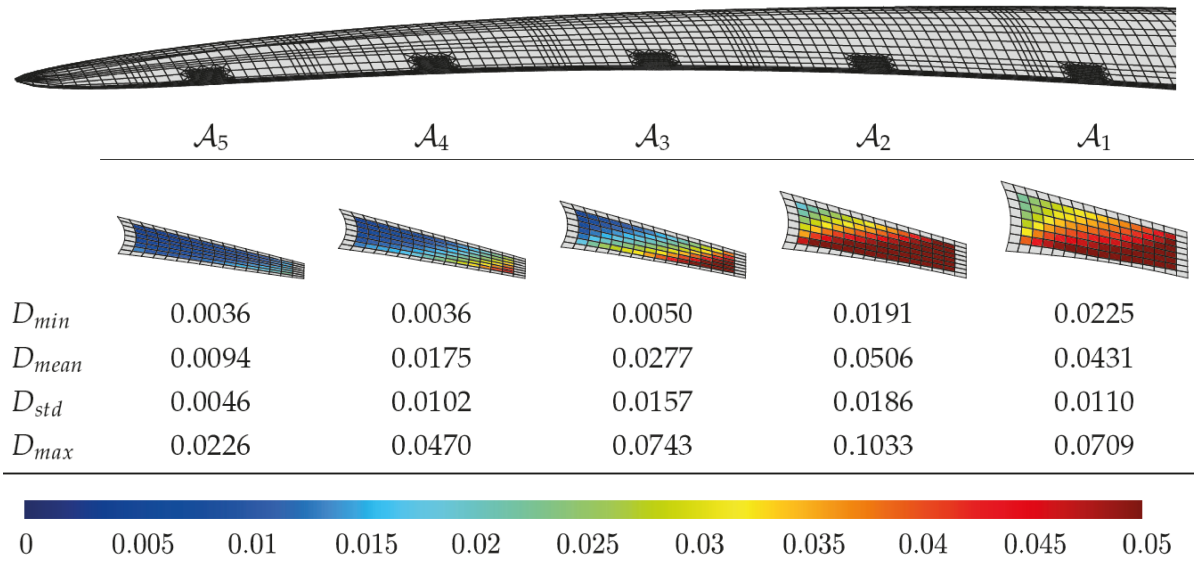

Figure 3: Fatigue damage results according to the critical plane approach using the Findley criterion (amplitude of the racetrack filter: 1000 Pa). The contours show the annual damages in the cross-sections located in the middle of the evaluation regions $\mathcal{A}_1$–$\mathcal{A}_5$. Statistical numbers are only valid for the plotted cross-sections. Since the interface between the adhesive and the adherends is not modelled, damages in the exteriour elements are not shown (D_{min}: minimum annual damage; D_{mean}: average annual damage; D_{std}: standard deviation of the annual damage; D_{max}: maximum annual damage).

numbers for the turbulent inflow, and inclined inflow situations with a yaw angle of $+8°$, $0°$, and $-8°$.

The contour plots show the annual damages on the critical planes in the cross-sections located in the middle of the different evaluation regions. We observe that the maximum damage is always located in the bottom right corner of the adhesive, which is due to the gouverning loading of unsymmetric bending. Hence, the simulation gives qualitatively a good picture of the fatigue processes in the adhesive.

Since wind turbines are designed for 20 years of operation, an annual fatigue damage should not exceed a value of $D_a = 0.05$. Otherwise, the adhesive will fail during the operation life of the turbine. However, for the evaluation regions $\mathcal{A}_1$–$\mathcal{A}_3$ we see annual damages of $D_{a3} = 0.0743$, $D_{a4} = 0.1033$, and $D_{a5} = 0.0709$, respectively. A re-design of the trailing edge could solve this problem. The major design parameter in this case is not the width of the adhesive joint (which is normally the design parameter in adhesive joints in applications different from wind turbine rotor blades) but the stiffness of the trailing edge spar cap. We have already verified that increasing the number of UD layers in the trailing edge spar cap reduces the annual damage of the adhesive joint to $D_a < 0.05$. The resulting increase in stiffness of the trailing edge structure leads to a lower level of longitudinal strain and consequently to a lower stress level in the joint.

In Fig. 4 we exemplarily show the annual damages for a typical finite element. We have plotted the annual damages on the analysed material planes on the corresponding segments of an adaptively discretised half sphere [26], see Fig. 4 (a). The underlying

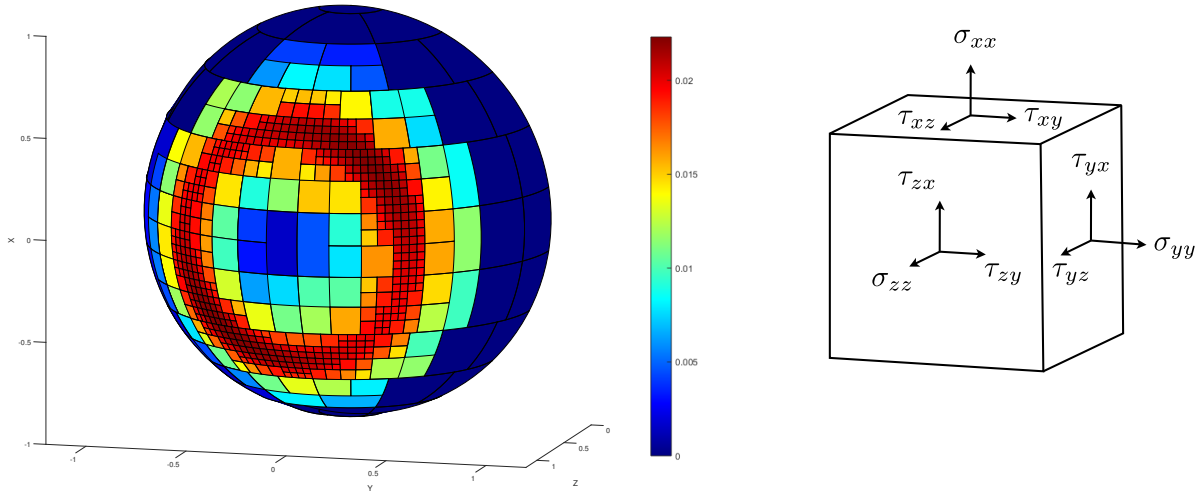

(a) (b)

Figure 4: Typical damage pattern for a critical plane fatigue analysis of the trailing edge adhesive joint of wind turbine rotor blades using the Findley criterion. Annual damages plotted on an adaptively discretised half sphere [26] that characterise the analysed material planes (a) and a sketch of the underlying coordinate system according to [2] (b).

coordinate system according to [2] is shown by means of the stress tensor components in Fig. 4 (b). The adaptive algorithm reduces the computational costs considerably, see [26].

Due to the dominant normal stresses in longitudinal direction compared with the shear stresses, an eye-like ring structure is established due to the Findley criterion, see Fig. 4 (a). If we only had shear stresses in the adhesive, the ring would be located at an opening angle of 45°, measured from the z axis. The Findley criterion looks for a linear combination of shear and normal stress. In the framework of a critical plane approach a maximisation of that linear combination is searched for. As a consequence, the opening angle of the ring decreases. In the particular example presented here, the opening angle is about 25°–30°.

5 CONCLUSIONS

In this paper, we presented one possible concept for ultimate strength and fatigue damage analyses for adhesive joints in wind turbine rotor blades. We described a finite element-based methodology for transferring internal forces and moments from a turbine simulation, which is usually based on beam models, into the stress space. This step is essential for strength analyses, as those are carried out on the basis of stress-strength relationships. We used 3D finite element simulations with appropriate load introduction techniques for this purpose. In particular, the concept of superposition of scaled unit load cases in the context of fatigue analyses has been pointed out.

A global equivalent stress approach incorporating the Drucker-Prager theory for ultimate strength analyses has been introduced. This approach accounts for multiaxial stress states as demanded by current design guidelines. Moreover, it includes different tensile and compressive normal strength parameters, which is an important feature capturing the properties of adhesives used in the wind energy industry.

A critical plane approach has been proposed for the fatigue damage calculation, because global equivalent stress approaches show weaknesses concerning non-proportional multiaxial stress histories. However, since rotor blades are subjected to a combination of deterministic and stochastic load influences, it is of high relevance to capture non-proportionality and multiaxiality. The critical plane approach maps the stress amplitude/mean stress/number of cycles combinations in the time histories by means of a multiaxial rainflow count.

The applicability of the proposed concept has been shown by a representative numerical example. The trailing edge adhesive joint of a reference rotor blade has been analysed and the results have been discussed in detail. It has been shown that it is essential to account for multiaxial stress states in an ultimate strength analysis. The importance to capture multiaxial non-proportional time histories in a fatigue analysis has further been elaborated.

The model shows qualitatively promising results. However, further strength criteria should be analysed in order to determine the impact of the chosen criteria. In the near future, experimental investigations are required for validation purposes, though these are difficult to carry out for non-proportional multiaxial stress states.

REFERENCES

[1] IEC 61400-1:2005(E). *Wind turbines - Part 1: Design requirements*. International standard. International Electrotechnical Commission, 2005.

[2] Germanischer Lloyd Industrial Services GmbH. *Guideline for the Certification of Wind Turbines*. Edition 2010. Renewables Certification, Hamburg, Germany.

[3] DNVGL-ST-0376. *Rotor blades for wind turbines*. Standard. DNV GL AS, 2015.

[4] Zarouchas, D. S., Makris, A. A., Sayer, F., van Hemelrijk, D., van Wingerde, A. M. Investigations on the mechanical behavior of a wind rotor blade subcomponent. *Composites Part B: Engineering* (2012) **43**(2):647–654.

[5] Eder, M. A., Bitsche, R. D., Nielsen, M. and Branner, K. A practical approach to fracture analysis at the trailing edge of wind turbine rotor blades. *Wind Energy* (2014) **17**(3):483–497.

[6] Eder, M. A. and Bitsche, R. D. Fracture analysis of adhesive joints in wind turbine blades. *Wind Energy* (2014) **18**(6):1007–1022.

[7] Rosemeier, M., Berring, P. and Branner, K. Non-linear ultimate strength and stability limit state analysis of a wind turbine blade. *Wind Energy* (2015) **19**(5):825–846.

[8] Noever Castelos, P. and Balzani, C. The impact of geometric non-linearities on the fatigue analysis of trailing edge bond lines in wind turbine rotor blades. Proceedings of the WindEurope Summit 2016. *Journal of Physics: Conference Series* (2016) **749**:012009 (pp. 1–10).

[9] Noever Castelos, P. and Balzani C. On the impact of multi-axial stress states on trailing edge bondlines in wind turbine rotor blades. Proceedings of The Science of Making Torque from Wind (TORQUE 2016). *Journal of Physics: Conference Series* (2016) **753**:062002 (pp. 1-10).

[10] Alejano, L. R. and Bobet, A. Drucker-Prager Criterion. *Rock Mechanics and Rock Engineering* (2012) **45**:995–999.

[11] Socie, D. F. and Talyor, G. B. *Multiaxial Fatigue*. Society of Automotive Engineers Inc., 1st Edition, 2000.

[12] Suresh, S. *Fatigue of Materials*, Cambridge University Press, 2nd edition, 2004.

[13] Haibach, E. *Betriebsfestigkeit- Verfahren und Daten zur Bauteilberechnung*, Springer-Verlag, 3rd Edition, 2006 (in German).

[14] Pinho de Castro, J. T. and Meggiolaro, M. A. *Fatigue Design Techniques Under Real Service Loads. Volume II - Low Cycle and Multiaxial Fatigue*. CreateSpace Indepentent Publishing Platform, 1st Edition, 2016.

[15] Miner, M. A. Cumulative damage in fatigue. *Journal of applied mechanics* (1945) **12**(3):159–164.

[16] ANSYS Inc. *ANSYS Mechanical APDL Theory Reference*, 2013.

[17] Larsen, T. J. and Hansen A. M. *How 2 HAWC2, the user's manual*, Risø-R-1597, Risø National Laboratory, 2015.

[18] Downing, S. D. and Socie, D. F. Simple rainflow counting algorithms. *International Journal of Fatigue* (1982) **4**(1):31–40.

[19] Wu, H., Meggiolaro, M. A. and Pinho de Castro, J. T. Validation of the multiaxial racetrack amplitude filter. *International Journal of Fatigue* (2012) **87**:167–179.

[20] Meggiolaro, M. A. and Pinho de Castro, J. T. An improved multiaxial rainflow algorithm for non-proportional stress or strain histories – Part II: The modified Wang-Brown method. *International Journal of Fatigue* (2012) **42**:194–206.

[21] Meggiolaro, M. A. and Pinho de Castro, J. T. An improved multiaxial rainflow algorithm for non-proportional stress or strain histories – Part I: Enclosing surface methods. *International Journal of Fatigue* (2012) **42**:217–226.

[22] Meggiolaro, M. A., Pinho de Castro, J. T. and Wu, H. Generalization of the moment of intertia method to estimate equivalent amplitudes for simplifying the analysis of arbitrary non-proportional multiaxial stress or strain histories. *Acta Mechanica* (2016) **227**:3261–3273.

[23] Wu, H., Meggiolaro, M. A. and Pinho de Castro, J. T. Application of the Moment Of Inertia method to the Critical-Plane Approach. *Frattura ed Integrità Strutturale* (2016) **38**:99–105.

[24] Findley, W. N. A Theory for the Effect of Mean Stress on Fatigue of Metals Under Combined Torsion and Axial Load or Bending. *Journal of Engineering for Industry* (1959), pp. 301-306.

[25] Weber, B., Kenmeugne, B., Clement, J. and Robert, J. Improvements of multiaxial fatigue criteria computation for a strong reduction of calculation duration. *Computational Material Science* (1999) **15**:381–399.

[26] Wentingmann, M. and Noever-Castelos, P. and Balzani, C. An adaptive algorithm to accelerate the critical plane identification for multiaxial fatigue criteria. *Proceedings of 6th European Conference on Computational Mechanics (ECCM 6) / 7th European Conference on Computational Fluid Dynamics (ECFD 7)*, 11-15 June 2018, Glasgow, UK.

[27] Teßmer, J., Icpinar, C., Daniele, E., Riemenschneider, J., Hölling, M. and Balzani, C. Schlussbericht Projekt Smart Blades, German Aerospace Center (DLR), 2016 (in German).

[28] Sevinc, A., Rosemeier, M., Bätge, M., Braun, R., Meng, F., Shan, M., Horte, D., Balzani, C., Reuter, A., Bleich, O., Daniele, E., Thomas, P. and Popko, W. IWES Wind Turbine IWT-7.5-164 Rev. 2.5. Fraunhofer IWES, 2017.

[29] Zarouchas, D. and van Hemelrijck, D. Mechanical characterization and damage assessment of thick adhesives for wind turbine blades using acoustic emission and digital image correlation techniques. *Journal of Adhesion Science and Technology* (2014) **28**(14–15):1500–1516.

[30] Issler, L., Ruoß, H. and Häfele, P. *Festigkeitslehre – Grundlagen*. Springer Berlin, 2nd Edition, 2006 (in German).

[31] Wacker, G. and Hauschildt, M. *Klebverbindungen in Rotorblättern für Windenergieanlagen*. Germanischer Lloyd, Hamburg, 2003 (in German).